JOURNAL OF MATERIALS SCIENCE **39** (2004) 619–630

A microstructural and mechanical study on the effects of carbon ion implantation on zirconia-toughened-alumina

M. E. MURPHY*, G. M. INSLEY
Scientific Affairs Research Group, Stryker Howmedica Osteonics, Limerick, Ireland
E-mail: matthew.murphy@emea.strykercorp.com

M. T. LAUGIER
Department of Physics, University of Limerick, Limerick, Ireland
E-mail: michael.laugier@ul.ie

D. SUTTON, S. B. NEWCOMB
Materials and Surface Science Institute, University of Limerick, Limerick, Ireland

Biomedical grade (>99.97% purity) alumina, zirconia and zirconia-toughened-alumina (ZTA) have been implanted with carbon ions at a dose of 5×10^{17} C ions/cm^2 using an ion energy of 75 keV. The near-surface hardness of these bioceramics was examined using a load partial-unload indentation technique, both before and after implantation. The surfaces of the bioceramics have also been examined in cross-section using transmission electron microscopy (TEM) both before and after implantation and the implantation data correlated with a computer based simulation, TRIM (Transport and Range of Ions in Matter). The grinding and polishing treatment used prior to the implantation treatment has been found to have a strong influence on the surface microstructures for all three ceramics, although more significant modifications are brought about by carbon ion implantation. A comparison was made between the near-surface hardness of the unimplanted and carbon ion implanted surfaces of these bioceramics with relation to the modified microstructure. TEM examination of the implanted surfaces has demonstrated the formation of a sub-surface amorphous layer in all three materials as well as other microstructural modifications, such as microcracking and an increase in the near-surface dislocation density, that are characteristic of ion damage. The hardness data reveals that carbon ion implantation tends to decrease the surface hardness of alumina and zirconia with increasing ion dose, with a significant decrease occurring at the immediate near surface for both materials.

1. Introduction

The excellent wear behaviour [1] and high strength [2] of high purity alumina ceramics has led to their widespread use in biomedical applications for a number of years [1, 3]. Such usage is limited by the inherent brittle nature of alumina [4] and for this reason there has been considerable interest in the development of less brittle materials in which the favourable high strength and wear properties are not significantly compromised. Zirconia, for example, has a higher bending strength and fracture toughness than alumina [1, 5] and this led to the development and use of zirconia based ceramics for biomedical applications in the mid-eighties [6]. However, the degradation of zirconia in which a tetragonal-to-monoclinic phase transformation is accelerated in aqueous environments [7–10] has severely restricted its use in biomedical applications. The lack of stability of the tetragonal zirconia phase has been found to be the cause of tribological failures in zirconia-on-zirconia bearing couples [6]. Such shortcomings initiated experimentation with alumina/zirconia composites [6] in order to take advantage of the hardness and wear properties of alumina as well as the favourable toughness and fatigue strength of zirconia. Zirconia-toughened-alumina (ZTA) has exhibited considerable early promise [11] and now looks set to be one of the next generation of biomaterials for use in joint replacements.

There remains scope for improvement in the properties of the ceramics currently used in biomedical applications. One technique by which the required improvement might be achieved is through the use of ion

*Author to whom all correspondence should be addressed.

implantation [12]. Ion implantation results in the near-surface modification of the implanted material through the introduction of pre-selected ions whilst leaving the bulk properties unchanged [13], and has been shown, for example, to have beneficial effects on both the fracture toughness and hardness of ceramics such as alumina [14, 15] and silicon nitrides [16]. Previous research has reported that the microstructural modification of alumina by carbon ion implantation improves tribological performance through the formation of a graphitic carbon structure at the surface of the alumina [17]. The aim of the study described here has been to examine the effects of carbon ion implantation on the nanohardness of biomedical grade ZTA and to correlate any mechanical modification to the near-surface microstructure of the treated ZTA. The approach taken has been to characterise ion induced modifications in the microstructure and hardness of the ceramic through a comparison of implanted and unimplanted surfaces. Any synergism between the effects of zirconia and alumina in the ZTA has been assessed through comparison of the microstructures of the surfaces of implanted and unimplanted alumina and zirconia samples. A computer based simulation (TRIM) has been used to provide a correlation between both the hardness data and the TEM observations of the near-surface microstructures with quantitative simulations of the depth distributions of the implanted carbon ions.

2. Experimental methods

The surfaces of polycrystalline biomedical grade (>99.97% purity) alpha-alumina, tetragonal-zirconia and ZTA were prepared using standard biomedical grinding and polishing methods [18] giving an R_a (arithmetic average roughness) value of <0.02 μm—a value that is required for bioceramics used in bearing applications. The ZTA samples consisted of a mixture of alpha-alumina and tetragonal-zirconia with a ratio of 75:25 (weight%) of alumina to zirconia. Carbon ion implantation was performed using a Danfysik 1090-200 high current implanter (Danfysik, Jyllinge, Denmark), using monocharged carbon ions at an ion dose of 5×10^{17} C ions/cm^2 and a beam energy of 75 keV. Samples for TEM were prepared using standard focused ion beam (FIB) thinning techniques and examined in a JEOL 2000FX TEM.

The nanohardness of the implanted and unimplanted samples were measured using a NanoTest nanohardness tester (Micro Materials, Wrexham, UK) equipped with a Berkovich diamond indenter. The nanohardness was determined using a method previously described by Oliver and Pharr [19] from a 20 cycle load-partial-unload indentation. This method permitted the elastic and plastic components of indentation to be separated and the hardness to be calculated at each step as a function of depth. The loading and unloading rate was 1.46 mN/s and the holding period at each peak load was 10 s. The target unloading percentage was 10% of the current maximum load for that cycle (i.e., 90% unloading before re-loading). A software simulation based on the Monte Carlo technique (TRIM [20]) was used to approximate the distribution and range of the implanted carbon ions in the implanted materials. The ion depth and distribution simulations have been correlated with both the nanohardness and the TEM data.

3. Results and discussion

3.1. Alumina: unimplanted surface

All implantation parameters (with the exception of the ion dose) were kept constant throughout the carbon implantation of the biomedical grade alumina. Results obtained from 20 cycle load-partial-unload displacement plots of indentations made on the unimplanted and carbon implanted alumina at various ion doses are shown in Fig. 1c. From Fig. 1c the nanohardness of the unimplanted alumina can be observed to decrease with increasing depths beneath the surface. This change in hardness can be explained by the presence of residual stresses [21, 22] originating from microstructural damage within the near-surface region of the ceramic, due to the grinding and polishing processes used to prepare this sample [23]. Residual stresses generated by such preparation processes are generally compressive in nature [24] and as such, can influence the hardness of the near-surface layer, resulting in an apparent increase in the surface hardness compared to that of an unstressed material. Previous work in this field has reported that by annealing the polished alumina, any residual stresses present at the near-surface may be removed, or at least, their influence on the near-surface hardness reduced [25–27]. However, although the authors of this paper have recognised that annealing the alumina prior to implantation would reduce this type of mechanically-induced damage, it was decided not to anneal so that the results described here remain relevant to surfaces prepared for biomedical applications.

In order to understand the influence of carbon ion implantation on the mechanical properties of alumina, the ion-induced microstructural damage was investigated through the TEM examination of the surface region of high dose (5×10^{17} C ions/cm^2) carbon implanted alumina and comparisons made with unimplanted alumina. A typical region of the unimplanted surface of the alumina is shown in Fig. 1a, which is a low magnification bright field image. The upper surface of the alumina has been capped by the high atomic number layer marked at A so as to protect the surface during the TEM specimen preparation thinning process. The bulk of the underlying ceramic can be seen to consist of equiaxed grains which vary in diameter from some 1.2 to 3 μm. Both intra and inter-granular pores are seen to be present (marked at B, C and D) but there is no evidence to indicate that the prior grinding treatment used on the alumina has promoted their formation. Instead, the formation of these pores occurred during the initial processing and sintering of the alumina powder to form the polycrystalline discs investigated here.

The upper regions of the alumina were examined in detail and the area marked at E in Fig. 1a is shown at a higher magnification in dark field in Fig. 1b. This micrograph was taken with the bulk of the alumina grain in a weakly diffracting condition and it was found that there is a clear tendency for such near-surface regions of the unimplanted material to be heavily strained (as at K

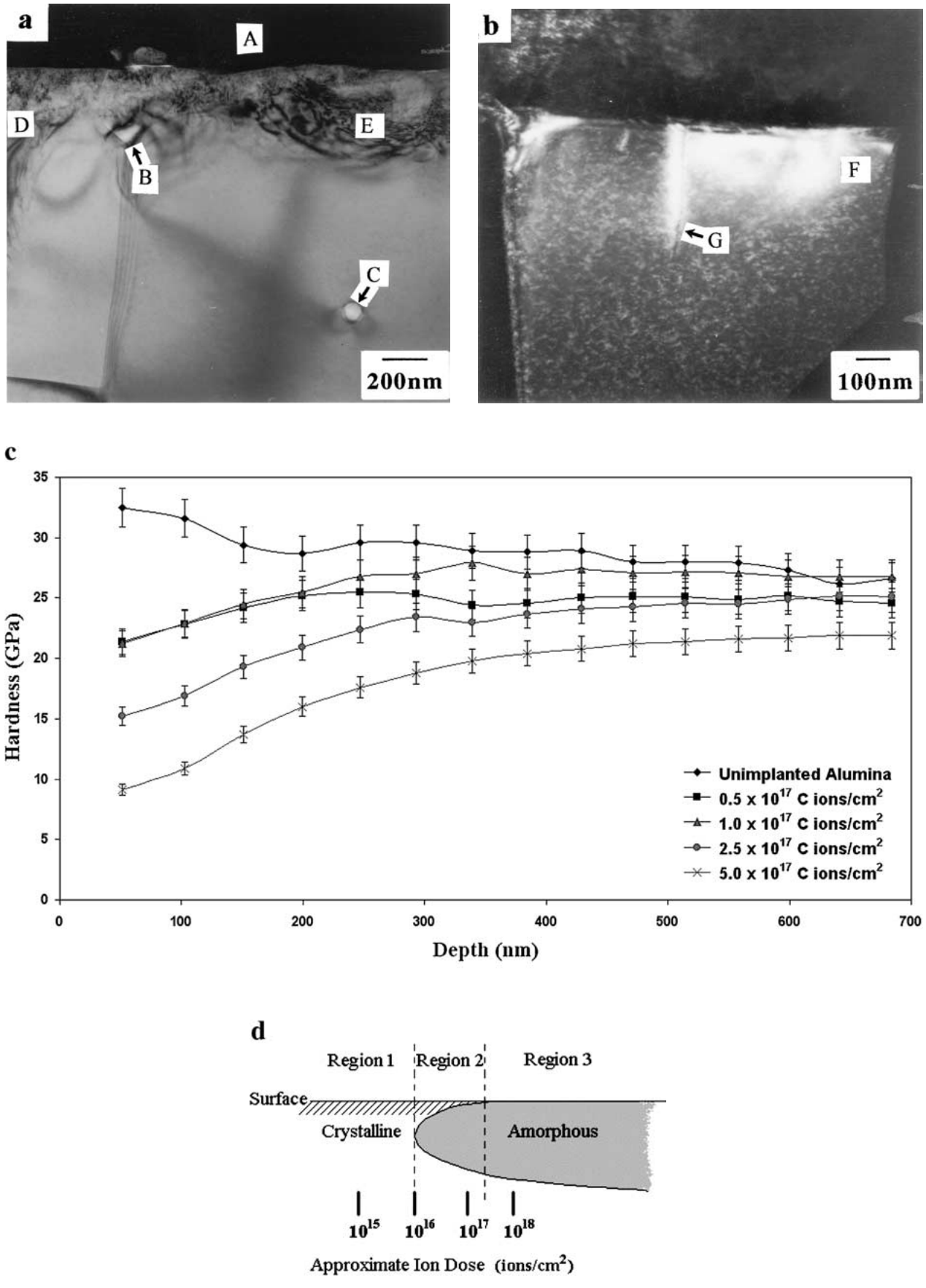

Figure 1 (a) Bright field and (b) higher magnification dark field micrographs showing the microstructures of a near-surface region of the unimplanted alumina whilst (c) displays variations in nanohardness with depth for unimplanted alumina and alumina surfaces implanted at doses of 0.5, 1, 2.5 and 5×10^{17} C ions/cm^2 and (d) is a schematic representation of the three primary microstructural regimes that can occur from ion implantation into crystalline materials [30].

in Fig. 1b). Further evidence that surface deformation has taken place is provided by the presence of dislocations (as at L) within the near-surface grain, Fig. 1a indicating that such dislocations can extend to a depth of some 1.35 μm beneath the very upper surface of the ceramic. The upper surface region was of further interest for the way in which it was found to consist of an irregular band (varying in thickness from approximately 300 to 680 nm) of heavily dislocated grains, as can be seen at the regions marked at F, G, H and I in Fig. 1a. The high dislocation content of the region described has been formed during the grinding and polishing treatment that was used prior to implantation of the ceramic and this has been further verified through the examination of an alumina surface that had been given a post-grinding anneal at 1350°C for seven hours [28].

3.2. Alumina: implanted surface

From Fig. 1c, it can be observed that for any given carbon ion dose, the near-surface hardness of alumina falls with decreasing penetration depth. Such a fall in the near-surface hardness appears to be promoted with increasing ion doses. The result of this load-partial-unload indentation reveals a dose dependant relationship for the carbon implanted alumina samples. From Fig. 1c, the near-surface hardness can be seen to decrease with increasing carbon ion dose (for depths less than 200 nm), particularly for the higher doses used in this work ($\geq 2.5 \times 10^{17}$ C ions/cm^2). Previous studies in this area have reported that high dose implantation of carbon into alumina promotes the formation of an amorphous layer [29, 30]. The formation of such a layer would explain the decrease in nanohardness with increasing ion dose due to the amorphous layer being softer than crystalline alumina [25, 27, 31–33]. This finding is further supported by the findings of Bull and Page [34], who reported the hardness of this amorphous layer to be approximately 60% of that of the unimplanted material—a result that was observed in this study for doses $\geq 2.5 \times 10^{17}$ C ions/cm^2.

Fig. 1d is a schematic representation showing the influence of ion implantation on the microstructure of crystalline materials. In region one, low dose implantation can be seen to result in the formation of a damaged crystalline surface structure, similar to that created by grinding and polishing of the alumina surface. Region two shows the initial formation of a subsurface amorphous layer which increases in thickness until at a specific ion dose (dependent on a number of factors such as ion energy, composition of target material, ion type, etc.), the amorphous layer reaches the surface. This totally amorphous surface layer can be seen at region three in Fig. 1d. Therefore, from this diagram it can be observed that the carbon ion doses used in this study were sufficient to form an amorphous layer—the thickness of this layer being dependent on the ion dose used. Thus, it is the presence of this layer which results in the overall decrease in the nanohardness of the carbon implanted alumina. This statement is further backed by a study carried out by Burnett and Page [30] on the influence of carbon implantation on the near-surface hardness of sapphire. These authors reported that a maximum surface hardness occurred in the implanted sapphire at an ion dose of approximately 5×10^{15} C ions/cm^2, after which, the surface hardness decreased for increasing ion doses. Their explanation for the initial increase for doses $\leq 5 \times 10^{15}$ C ions/cm^2 was that low dose carbon implantation created a volume expansion in the implanted layer [35]. This volume expansion was due to both (a) the production of point defects (such as vacancy/interstitial pairs) in the crystal structure as a result of the displacement of atoms of the sapphire from their lattice positions, and (b) the presence of the implanted atoms at the near-surface, i.e., 'ion-stuffing' of the surface layer [30]. Since this modified layer is constrained by the underlying undamaged bulk material, large compressive stresses can be generated, resulting in an apparent increase in the near-surface hardness due to the resistance of the compressed layer to deformation by an indenter [27]. However, once the amorphous layer begins to form with increasing ion dose, the influence of these compressive stresses is gradually reduced by the presence of the softer amorphous layer [30, 34]. The mechanism by which partial stress relief occurs may be attributed to the softer amorphous layer expanding vertically in response to the biaxial lateral compressive stresses within it [35]. Burnett and Page suggested that this stress-relief (due to the formation of an amorphous layer) might indicate that the amorphous layer has a lower load-bearing capability compared to the crystalline material [30]. Hence, as the amorphous layer becomes thicker with increasing ion dose, it has an increased influence on decreasing the near-surface hardness of the implanted alumina, as can be seen in Fig. 1c.

Fig. 2a is a bright field micrograph which was taken from a typical region of the carbon implanted surface. The ion implantation of the alumina has led to a number of significant microstructural changes by comparison with the image shown earlier in Fig. 1a for the unimplanted surface. The upper surface of the ceramic has again been capped with a protective high atomic number layer (at M). As with the unimplanted alumina, the bulk of the ceramic was found to consist of reasonably coarse equiaxed grains that contain a number of inter and intra-granular pores, as typified by the defect marked at N in Fig. 2a. The region marked at O in Fig. 2a is shown in dark field in Fig. 2b, and from here two distinct regions can be identified. The upper region of the grain (as at U) contains a dense agglomerate of dislocations whilst the lower region (V) was found to have a dislocation microstructure that was consistent with a lower carbon ion dosage. Although the defects marked at V extended no more than approximately 1 μm beneath the surface of the ceramic, the density of such defects is clearly higher than in the unimplanted sample. The relationship between these two zones of different dislocation content is underlined by the fact that the highly defective band (at U) extended to a depth of some 575 nm beneath the upper surface of the sample, and from here, the defects at V were initiated. This observation contrasts with the unimplanted sample in

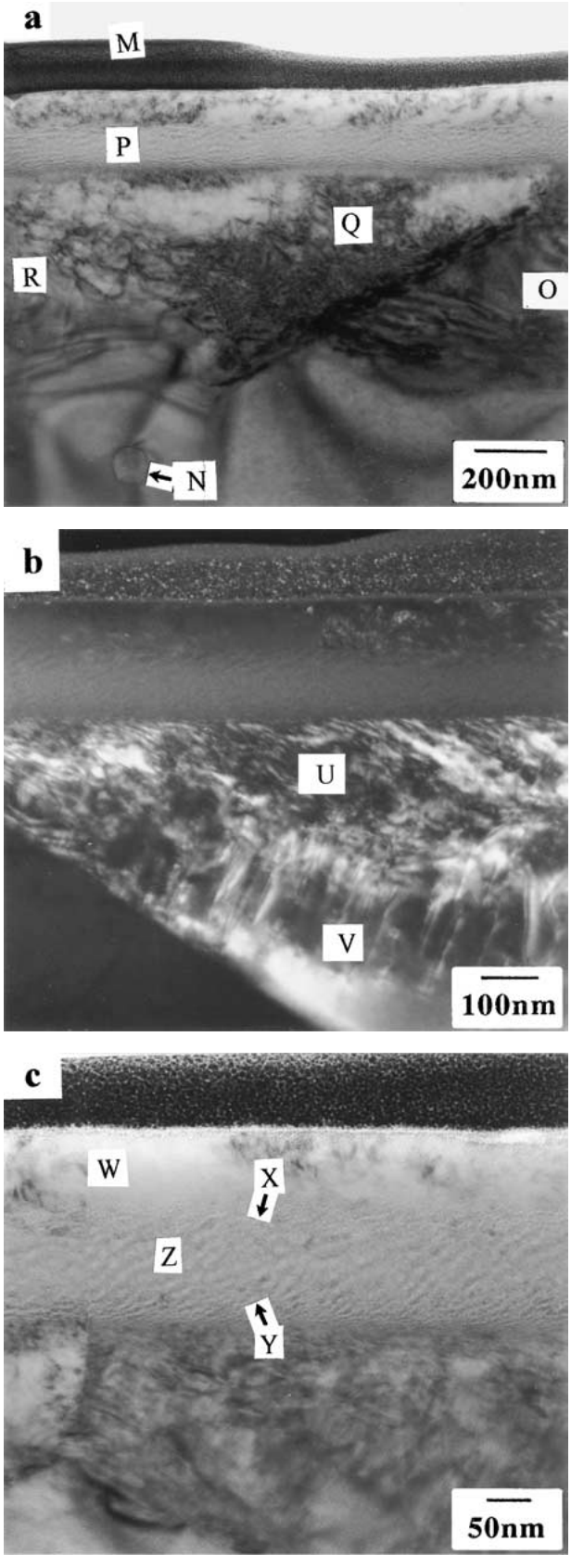

Figure 2 (a) Bright field micrograph of a near-surface region of alumina implanted with carbon ions at a dose of 5×10^{17} C ions/cm^2, whilst the region marked at O is shown in (b) as a dark field micrograph.

which the upper surface of high dislocation content was found to be rather variable (300–600 nm). Further evidence for the observations described comes Fig. 2a, where the upper band of high defect alumina is marked at Q and the defects that have been formed in the underlying grain can be seen particularly well at O, R, S and T.

The upper surface region of the ceramic was examined in further detail and the region marked at P in Fig. 2a is shown at higher magnification in Fig. 2c, which demonstrates the formation of a number of distinct regions. The surface of the ceramic contains both an amorphous band (as at W), which typically extends to a depth of some 75 nm, and an inhomogeneous distribution of fine, equiaxed crystallites (approximately 50 nm in diameter). Immediately beneath this upper band, a zone of amorphous material is found and this part of the structure extends to a depth of 225 nm beneath the upper surface of the alumina (between the points marked at X and Y in Fig. 2c). The contrast observed in the zones marked at X and Y in Fig. 2c, which was not seen in the more central parts of the amorphous zone (such as at Z), originates from elongated voids running parallel to the implanted surface. Closer examination of this region indicates that the two sub-bands consist of an amalgam of amorphous material and fine equiaxed grains. The critical point, however, is that the formation of this depth dependent layer is related to the lattice damage created by the implanted carbon ions. Such an amorphous zone is expected to form when the damage level in the collisions between the implanted ions and substrate atoms exceeds some threshold value [36].

Comparisons were made between the TEM observations, nanohardness data and TRIM simulations of the simulated distribution of implanted carbon ions in the alumina. Fig. 3a shows a TRIM simulation and indicates that the maximum concentration of carbon lies at a depth of some 140 nm beneath the surface of the alumina with a skewed Gaussian distribution in the ion concentration versus depth. It can be seen that implantation did not occur at depths greater than approximately 225 nm and that there is a distinct fall in the carbon ion concentration towards the surface of the alumina. Comparison of the TEM images with the TRIM data showed that the position of the maximum concentration of the implanted carbon ions lies at the centre of the amorphous zone described in Fig. 2c (at point Z). In addition, it can be seen that the half-height peak-width positions are very close to the boundaries marked at X and Y in Fig. 2c, above and below which the amorphous layer was found to be intermixed with very fine grains of alumina. The surface region in the simulated carbon ion distribution appears to correspond to the zone containing the alumina grains within the band marked at W in Fig. 2c.

By comparing these simulations with the nanohardness data, it can be observed that the depths at which the near-surface hardness was modified due to implantation corresponds to those depths at which TRIM predicted for the implanted carbon distribution, i.e. the nanohardness was found to be modified for depths up to approximately 300 nm. The close correlation between the simulated carbon ion distribution and the position of the amorphous zone is crucial in verifying the application of such simulations and thus how TRIM can be used to further the understanding of implantation-induced microstructural artefacts.

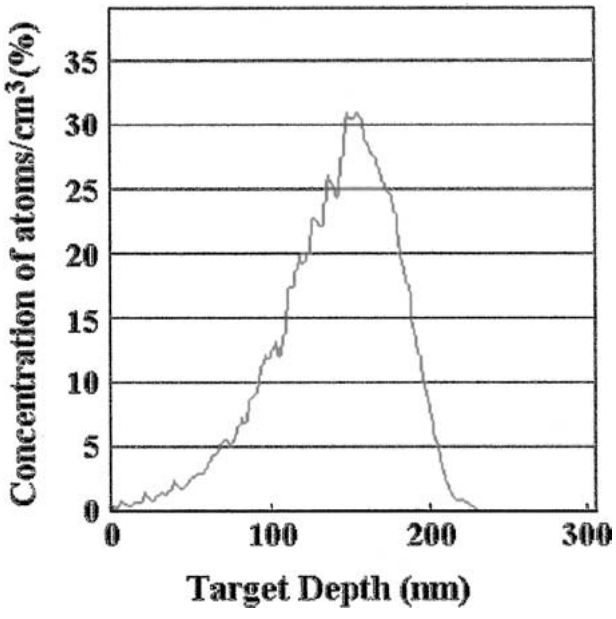

(a)

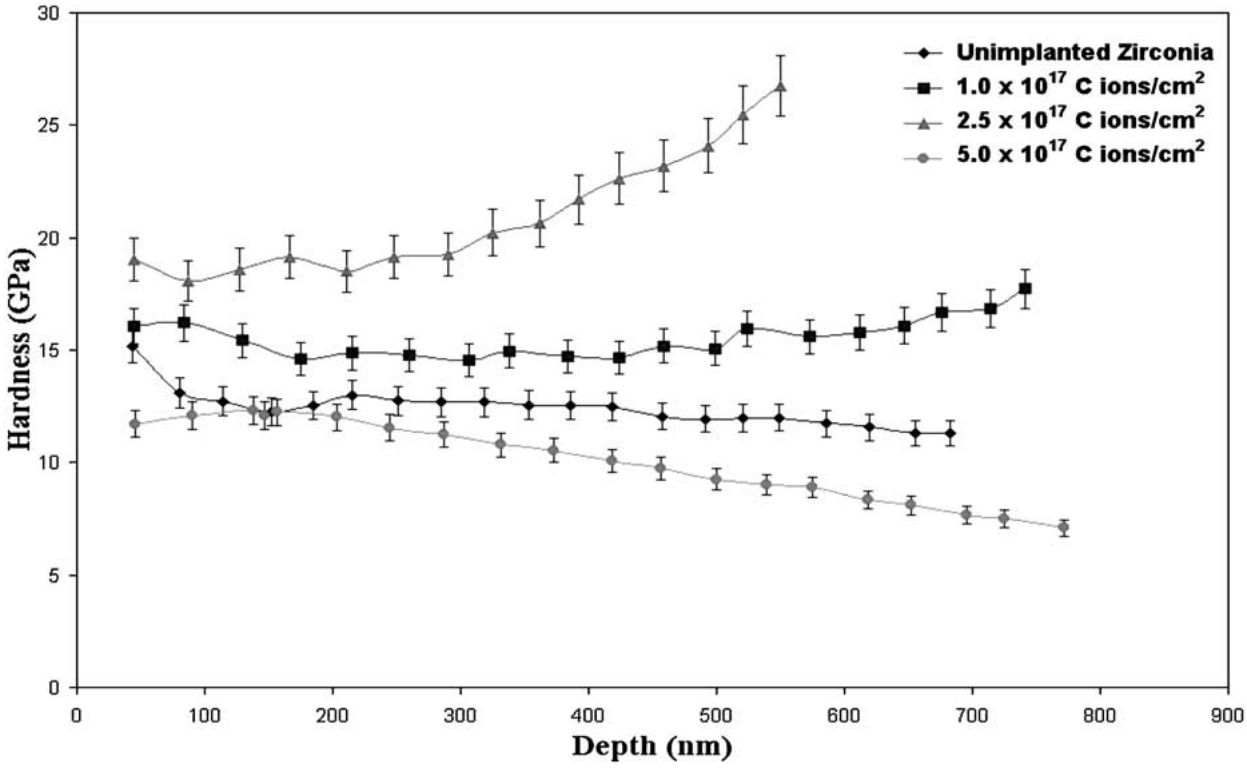

(b)

Figure 3 (a) TRIM simulated distribution of implanted carbon ions for a dose of 5×10^{17} C ions/cm^2, as a function of depth beneath the alumina surface, whilst (b) displays the variations in nanohardness with depth for carbon implanted and unimplanted zirconia surfaces implanted at doses of 1, 2.5 and 5×10^{17} C ions/cm^2.

3.3. Zirconia: unimplanted surface

Fig. 3b displays the change in nanohardness with depth for the unimplanted and carbon implanted zirconia samples. As for the unimplanted alumina (previously discussed), the nanohardness of the unimplanted zirconia was found to decrease with increasing depth beneath the surface. The increase in hardness at the near-surface can be attributed to microstructural damage to the zirconia surface from the grinding and polishing steps performed to prepare these samples [37, 38], see Fig. 4c where the presence of surface grinding induced deformation twins (as at F) can be detected.

A typical region of the zirconia that was thinned to electron transparency is shown at relatively low magnification in Fig. 4a. Here we are seeing a bulk region lying well beneath the polished surface. An equiaxed grain microstructure has been formed and it is immediately apparent that there is a significant degree of variability in the grain size of the oxide (0.2 to 0.7 μm). It is of further interest to note the presence of the fine pore that has been formed in the region intersecting the grain boundaries marked at A in Fig. 4a although it is emphasised that the volume fraction of such defects in this material was low. The equiaxed form of the oxide

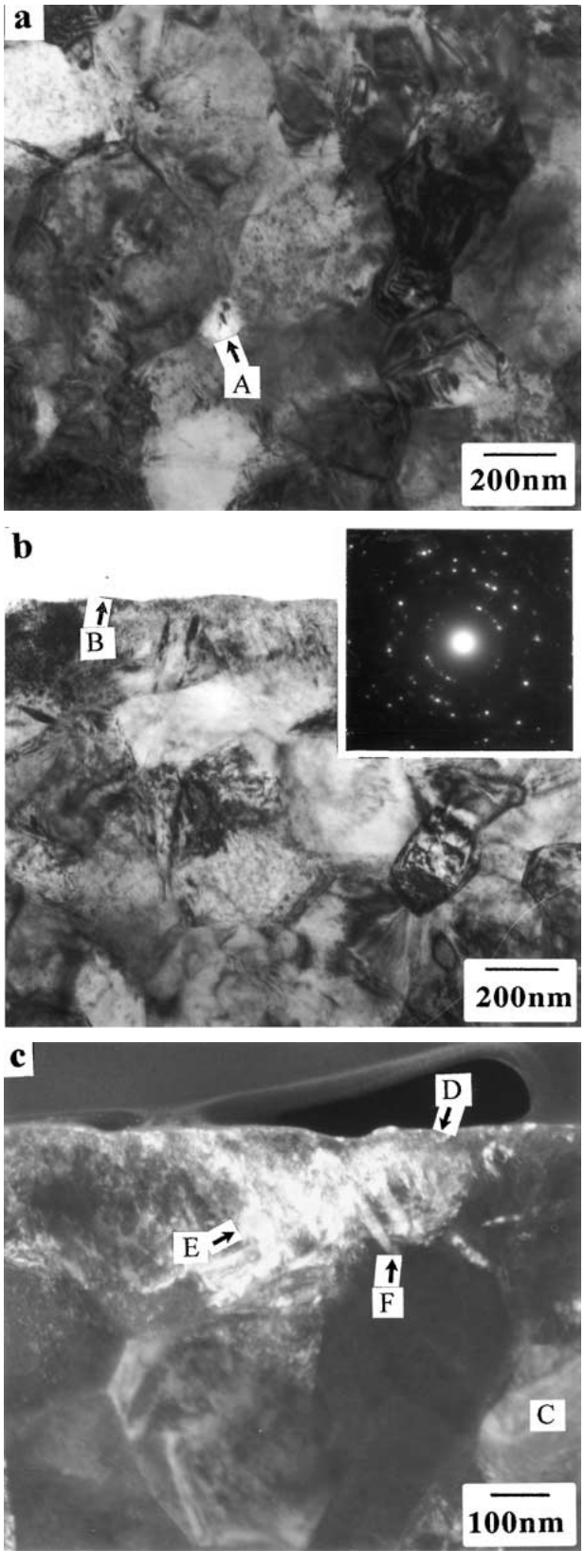

Figure 4 (a) Bright field micrograph of the bulk zirconia and (b) the unimplanted zirconia surface whilst (c) is a high magnification dark field micrograph showing the polishing-induced damage to the near-surface of the unimplanted zirconia.

grains is further underlined by the appearance of the selected area diffraction pattern (SAD), the ring spacings confirming the presence of the tetragonal nature of the zirconia (insert in Fig. 4b). It was also observed that some of the image contrast originates from FIB thinning damage that has occurred during the sample preparation (C in Fig. 4c), whilst in other areas a number of defects can be seen which can be directly related to the grinding and polishing procedures, such as the fine irregularities marked at D and E in Fig. 4c. In this respect, the dislocation content of the oxide appears to be significantly higher than was seen in the bulk regions of the previously examined unimplanted alumina.

The polished surface of the unimplanted zirconia was similarly investigated and a typical region is shown in Fig. 4b. The surface of the sample has been marked at B and it is interesting to note that the prior grinding and polishing treatment has resulted in a number of microstructural changes. A high magnification dark field image of the oxide surface is shown in Fig. 4c and from here, the presence of surface grinding induced deformation twins (as at F) can be observed. The formation of such twins—which extend to depths of 100 to 250 nm beneath the surface of the oxide—is paralleled by the high dislocation content of the surface zirconia grains (as at E), but there was no evidence for the formation of the monoclinic phase.

3.4. Zirconia: implanted surface

Carbon implantation using an ion dose of 1×10^{17} C ions/cm^2 resulted in an overall increase in the near-surface hardness of treated zirconia, see Fig. 3b. Further implantation at a dose of 2.5×10^{17} C ions/cm^2 caused the near-surface hardness to increase further, whilst implantation using 5×10^{17} C ions/cm^2 resulted in an overall decrease in the nanohardness of the implanted zirconia. This initial increase can be explained by the accumulation of residual stresses at the surface by the formation of point defects and a highly dislocated near-surface microstructure [38]. Further implantation using a dose of 2.5×10^{17} C ions/cm^2 caused the near-surface hardness to increase further by increasing the defect concentration at the near-surface. However, once a dose of 5×10^{17} C ions/cm^2 was used, the near-surface hardness decreased because of the surface-softening effect that the formation of an amorphous layer produces [39]. Previous implantation studies have demonstrated that zirconia is one of the most radiation-induced-damage resistant ceramics [40, 41]. Sasajima *et al.* [41] have classified zirconia as an oxide that is among the most resistant ceramics to irradiation-induced amorphisation based on its high bonding ionicity. It is this inherent property that imparts high mobility to its constituents and promotes defect recombination and precipitation which limits the build-up of defects or impurity concentrations required for total amorphisation [42]. Thus, implantation of zirconia using an ion dose of 5×10^{17} C ions/cm^2 produced a partially-amorphous surface layer with remnants of the original crystalline structure, as can be seen from the residual grain boundary at M in Fig. 5b. In addition, the nanohardness of the 2.5×10^{17} C ions/cm^2 implanted sample can be observed to increase considerably for depths $\geq$300 nm, see Fig. 3b. A similar trend can be detected for the 5×10^{17} C ions/cm^2 implanted zirconia sample at depths $\geq$550 nm. A similar phenomena has been reported by Boudoukha *et al.* [38] where they reported that "a dispersion of experimental

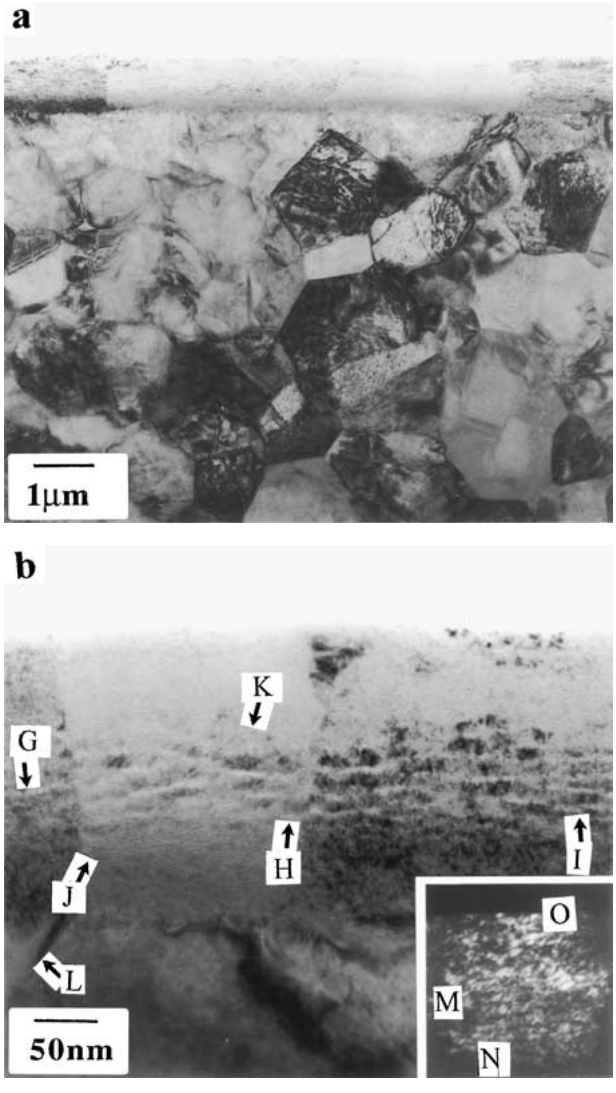

Figure 5 Bright field micrographs, (a) and (b) showing modification of the near-surface zirconia grains after carbon implantation (5×10^{17} C ions/cm^2).

values occurs, that can be related to the presence of grain boundaries. . . ". This statement is further supported by the grain size distribution of this zirconia being 0.39 ± 0.15 μm [43]. Therefore, it is quite reasonable to assume that a grain boundary was encountered at a depth of approximately 300 nm with the 2.5×10^{17} C ions/cm^2 implanted sample and approximately 550 nm for the 5×10^{17} C ions/cm^2 implanted sample, thus resulting in the observed increase in the nanohardness of these samples at the depths specified.

A typical region of the carbon implanted zirconia is shown at a relatively low magnification in Fig. 5a and it is immediately apparent that the surface treatment has led to a significant change in the near surface microstructure of the oxide. A higher magnification bright field image is shown in Fig. 5b, and this makes an interesting comparison with the previously examined carbon implanted alumina surface. Here the equiaxed grain microstructure of the zirconia has been retained in the upper regions of the sample with the formation of a number of porous bands within the surface modified layer. Such bands can be seen at positions such as those marked at G, H and I, the widths of the bands being at their highest towards approximately the centre of the modified layer. Finer bands of pores are visible at the position marked at J, which lies at a depth of approximately 245 nm from the surface of the sample. The upper parts of the layer were found to contain a distribution of spherically shaped voids (as at K in Fig. 5b) although the volume fraction of such defects tended to fall at the very upper surface of the sample. The generally crystalline nature of the upper parts of the implanted zone is further underlined by the form of the inset dark field image shown in Fig. 5b, in which a vertical grain boundary can be observed to pass through the modified zone (as at M). This dark field image also demonstrates that the formation of the porous zones has led to the partial microstructural disruption of the oxide grains and that there is a tendency for small localised misorientations to have been formed. The latter aspect of the characterisation is again typified by the inset dark field in Fig. 5b, in which an example of a locally misoriented grain has been marked at N. There is a further tendency for the very upper surface of the implanted surface to consist of a fine band (20 nm in thickness) of material in which the grain misorientation is even higher: this type of band has been marked at O. Fig. 5b is of further interest with regard to the microstructure of the zirconia situated immediately beneath the modified band, which was found to be decorated with a number of twins (as at L). These twins were found to extend to a depth of some 500 nm beneath the surface of the sample and in this way appear to be rather more developed as a result of the carbon implantation than those formed during the prior grinding and polishing treatment.

A TRIM simulated distribution of implanted carbon ions in zirconia for an ion dose of 5×10^{17} C ions/cm^2 and a beam energy of 75 keV is shown in Fig. 6. The TRIM simulation indicates that the maximum concentration of the implanted ions occurred at a depth of approximately 130 nm beneath the surface of the zirconia. The implanted ion distribution was found to have a

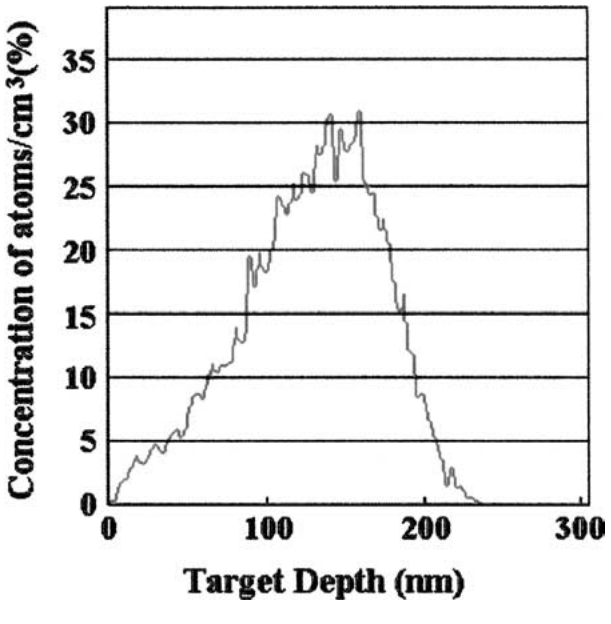

Figure 6 Simulated distribution of the implanted carbon ions for a dose of 5×10^{17} C ions/cm^2, as a function of depth beneath the zirconia surface.

near-Gaussian distribution and to be generally similar to that seen for the implanted alumina. Implantation does not occur at depths greater than approximately 220 nm and there is a decrease in the number of carbon ions towards the surface of the zirconia. As for the implanted alumina, it was found that the position of the maximum concentration of the implanted carbon ions in zirconia lies at the centre of the amorphous zone described in Fig. 5b (at point H). In addition, the region within the half-height peak-width of the TRIM plot contains the porous bands such as those labelled at G, H and I. The TRIM simulations were found to correspond to the nanohardness data obtained for these samples, i.e., with the exception of the increase in the hardness of the 2.5×10^{17} C ions/cm^2 sample due to the probable presence of a grain boundary, the most significant changes in the near-surface hardness of the implanted zirconia were at depths $\leq$250 nm. There would thus appear to be a close correlation between the TRIM simulated carbon ion distribution, the TEM observations of the implanted surface and the nanohardness data.

3.5. Zirconia toughened alumina: unimplanted surface

Nanohardness testing of the ZTA samples used in this study was not possible due to the inability to visibly distinguish (and therefore position the nanohardness indenter) between zirconia and alumina grains. However, previous studies [43] involving microhardness testing of the ZTA used in this study reported a hardness of 21.4 GPa for alumina, 13.4 GPa for zirconia and 21.5 GPa for ZTA, respectively. Such results indicate that ZTA appears to retain the hardness of its main constituent ceramic, i.e. alumina. Therefore, it is reasonable to assume that the nanohardness of the implanted alumina and zirconia grains in the ZTA would be similar to that of the nanohardness for 'pure' alumina and zirconia both before and after implantation at various carbon ion doses.

Part of the ZTA sample that was thinned to electron transparency is shown in Fig. 7a which is a relatively low magnification bright field image. Much of the sample is made up of alumina grains, with a uniform distribution of zirconia being present in a lower volume fraction, as indicated by the grains marked at A and B. The zirconia grain at C intersects the polished surface of the sample and such grains are thus of particular interest. The alumina grains, by comparison, were found to be generally of a smaller diameter than the 1.2 to 3 μm grains seen in the 'pure' alumina sample and were also found to be of a lower dislocation content. The zirconia grains are similarly faceted and although much of the image contrast originates from unavoidable FIB damage incurred during the TEM sample preparation, the grains are of a higher defect content than the alumina. The sample was found to contain a small number of pores and an atypical locally high density can be observed in Fig. 7a at D, and although these are lying in close proximity to the surface of the sample it remains unlikely that their formation has been initiated by the prior mechanical treatment given to the surface of the ZTA. As for the 'pure' alumina samples, the formation of such pores is more likely to have taken place during the initial processing and sintering of the ZTA powder. A grain boundary pore can similarly be seen at E and this time it lies at the intersection of alumina and zirconia grains.

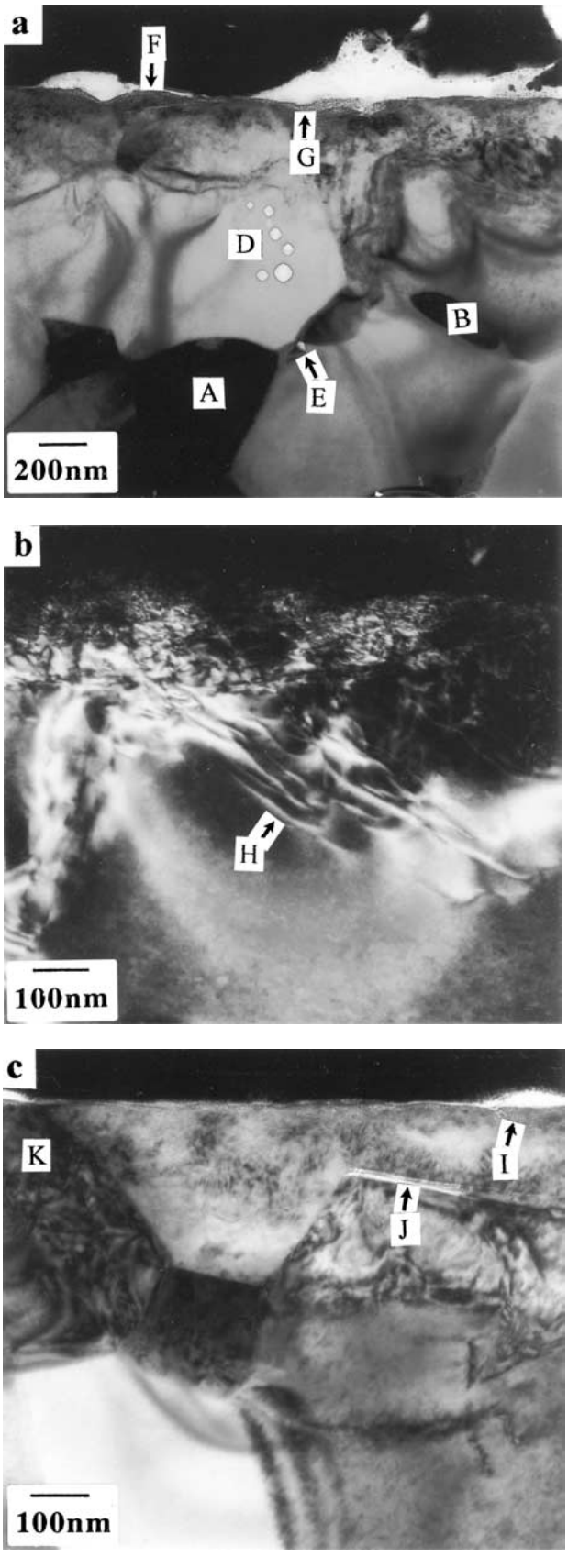

Figure 7 (a) Bright field micrograph of the unimplanted ZTA surface, whilst (b) and (c) are dark and bright field micrographs displaying the dislocation content of the near-surface produced by sample preparation.

The surface regions of the ZTA were examined in detail and it should be noted that the dislocation content of the near-surface alumina is significantly higher than in those grains situated further from it. Evidence for this observation comes from the dislocations observed in the dark field image shown in Fig. 7b at H and the grain microstructure appears to be consistent with that described earlier for the polished surface of the alumina. In this way a high density of dislocations can be seen to extend down to a depth of some 300–600 nm from the surface (surface is at G). Fig. 7a is of further interest for the localised nature of some of the changes that have occurred at the very upper surface of the alumina during the prior grinding and polishing treatment with the formation of the highly porous band marked at F and G. The depth of this porous zone clearly exhibits significant variations across the surface, particularly at the surface grain boundaries (as at F). Further evidence for these observations comes from the bright field micrograph shown in Fig. 7c in which the high defect content of the surface can be clearly seen, as at I. A large crack has formed between two alumina grains (at J) and it is again noted that the grain immediately beneath this defect contains a characteristic array of dislocations that extends down to a depth of some 600 nm from the surface. This region contains a zirconia grain marked at K and it is significant that the very upper regions of this part of the structure were found not to contain any localised cracks or pores. There was no evidence, however, to indicate that the formation of the crack at J was initiated by a tetragonal-to-monoclinic transformation of the tetragonal zirconia grain marked at K.

3.6. Zirconia toughened alumina: implanted surface

Fig. 8a is a bright field micrograph taken from a typical region of the ion implanted ZTA surface. Carbon implantation has led to a number of significant microstructural changes in the ZTA when comparisons are made with the unimplanted surface shown earlier in Fig. 7a. The microstructural changes that have occurred within the alumina lying at either side of the zirconia grains marked at L and M are broadly similar to those described previously for the 'pure' alumina, and for this reason are not described in detail again. The bright field image in Fig. 8b further underlines the similarity between the implanted alumina and

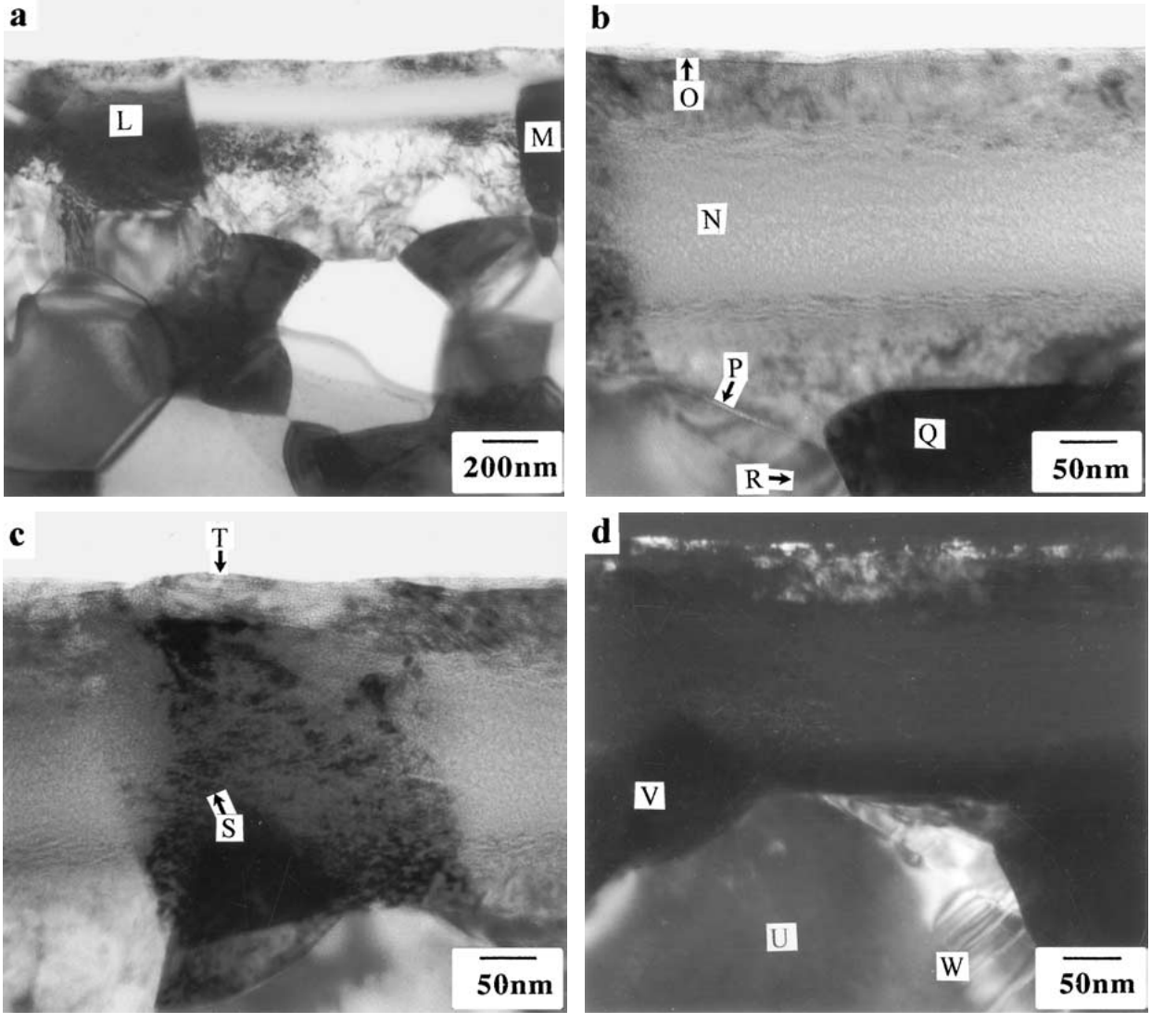

Figure 8 Bright field, (a) and (c) and dark field micrographs (b) and (d) of the carbon implanted ZTA surface displaying the amorphisation and cracking of the near-surface after implantation.

implanted alumina grains in the ZTA, by the formation of a broad band of amorphous material at N, which is capped by the layer of relatively fine grains marked at O. Fig. 8b also demonstrates the formation of a fine crack in the alumina grain lying just to the side of the zirconia marked at Q. The latter was found to be tetragonal, and there is thus no evidence that the formation of the crack was initiated by the volume changes associated with a tetragonal-to-monoclinic transformation [44]. Unlike previous investigations in which such a transformation has been found to be promoted by either thermal treatments [6] or an applied stress [45], any compressive stresses generated within the near-surface regions of the sample during ion implantation are apparently not high enough for this to have occurred. Stress does however appear to have played some role in the microstructural development of the surface of the ZTA given the appearance of the dislocation array in the alumina grain marked at R in Fig. 8b.

Fig. 8c is a bright field image which partially demonstrates the formation of bands within the zirconia (as at S) in ways that are generally similar to those described above for the 'pure' zirconia based sample. Here, the zirconia grain lies beneath a 40 nm band of material marked at T and in this way it would appear that the zirconia did not extend to the very upper surface of the sample given that we are seeing a thin capping layer of fine grained alumina. In this context, it is interesting to find that the alumina (at U) lying immediately beneath the zirconia grain (at V in Fig. 8d) is of low defect content by comparison with the region lying to its side (at W). This observation is significant because the zirconia would appear to be able to 'absorb' some of the applied stresses, so increasing the overall apparent toughness of the composite. The near-surface modification of the ZTA brought about by carbon implantation is clearly highly dependent on the identity of those grains lying at its very upper surface, although the microstructural changes themselves are very similar indeed to those seen in two non-composite materials. There is, however, some additional synergism in the effects of the alumina and zirconia within the ZTA and this too is reflected in some of the observed near-surface microstructures, i.e., cracking of alumina adjacent to zirconia grains, see Fig. 8b.

4. Conclusions

The effects of carbon ion implantation on the surface microstructure of biomedical grade ZTA have been investigated using TEM in relation to the influence of implantation on 'pure' alumina and zirconia and the consequence of combining these ceramics. It has been found that for any given carbon ion dose used in this study (5×10^{16} to 10^{17} C ions/cm^2), the near-surface hardness of alumina falls with decreasing penetration depth and that this reduction in hardness increases with increasing ion dose. From this study, it was been found that this reduction in hardness was directly related to the thickness of the ion damaged near-surface layer which was found to increase with increasing ion dosage. By comparison of TEM results against TRIM simulations, it was found that the depths at which the near-surface hardness was modified due to implantation corresponded directly to those depths at which TRIM predicted for the implanted carbon distribution. Thus, high-dose carbon ion implantation (5×10^{17} C ions/cm^2) of alumina resulted in the formation of an amorphous, near-surface layer which extended to a depth of approximately 225 nm beneath the surface.

The formation of such an amorphous layer was also found to occur in the surface zirconia grains (using the same carbon ion dose) to a depth of approximately 220 nm beneath the implanted surface. No evidence of tetragonal-to-monoclinic transformation in the ZTA after implantation was detected. Implantation of zirconia using an ion dose of 5×10^{17} C ions/cm^2 produced a partially amorphous surface layer with remnants of the original crystalline structure still being visible. The near-surface hardness of zirconia was found to increase with increasing carbon ion dosage to a dose of 2.5×10^{17} C ions/cm^2 before decreasing with further increases in the ion dose. This decrease for the higher ion doses can be related to the formation of ion-induced damage to the near-surface and a resultant softening of this damaged layer.

The experiments presented in this research for alumina and zirconia were necessary to describe the interaction between these two ceramics when combined in ZTA as well as the influence of carbon implantation on this material. TEM analysis of the ZTA near-surface displayed the inherently tougher zirconia apparently 'absorbing' any ion-induced stresses, whilst the more brittle nature of alumina was revealed by the formation of fine cracks and the presence of dislocations in an attempt to relieve such stresses. It was observed that the carbon implanted near-surface microstructure, i.e. ion depth and distribution of the carbon ions in ZTA resembled that of both its constituent materials, depending on the composition of the surface grain examined.

Acknowledgements

Financial support by an Enterprise Ireland Strategic Research Grant, under Contract No. ST/98/423 is gratefully acknowledged. The authors wish to thank Professors D. N. Buckley and B. K. Hodnett for the provision of laboratory facilities.

References

1. J. M. DORLOT, P. CHRISTEL and A. MEUNIER, *J. Biomed. Mat.* **23** (1989) 299.
2. D. MUNZ, R. T. BUBSEY and J. L. SHANNON, *J. Amer. Ceram. Soc.* **63** (1980) 300.
3. C. PICONI, M. LABANTI, G. MAGNANI, M. CAPORALE, G. MACCAURO and G. MAGLIOCCHETTI, *Biomaterials* **20** (1999) 1637.
4. A. MUCHTAR and L. C. LIM, *Acta Mater.* **46** (1998) 1683.
5. G. WILLMANN, *Bioceramics* **6** (1993) 38.
6. C. PICONI and G. MACCAURO, *Biomaterials* **20** (1999) 1.
7. R. C. GARVIE, C. URBANI, D. R. KENNEDY and J. C. McNEUER, *J. Mat. Sci.* **19** (1984) 3224.
8. Y. MURASE and E. KATO, *J. Amer. Ceram. Soc.* **66** (1983) 196.
9. S. AFFATATO, M. GOLDONI, M. TESTONI and A. TONI, *Biomaterials* **22** (2001) 717.
10. J. F. LI and R. WATANABE, *J. Amer. Ceram. Soc.* **81** (1998) 2687.

11. Y. J. HE, A. J. WINNUBST, A. J. BURGGRAAF, H. VERWEIJ, P. G. VAN DER VARST and G. DE WITH, *J. Eur. Ceram. Soc.* (1997) 1371.
12. F. Z. CUI and Z. S. LUO, *Surf. Coat. Technol.* **112** (1999) 278.
13. J. RIEU, A. PICHAT, L. M. RABBE, A. RAMBERT, C. CHABROL and M. ROBELET, *Mater. Sci. Technol.* **8** (1992) 589.
14. P. J. BURNETT and T. F. PAGE, *J. Mater. Sci.* **19** (1984) 3524.
15. F. HALITIM, N. IKHLEF, L. BOUDOUKHA and G. FANTOZZI, *Thin Solid Films* **300** (1997) 197.
16. F. BRENSCHEIDT, W. MATZ, E. WIESER and W. MOLLER, *Surf. Coat. Technol.* **110** (1998) 188.
17. J. TIAN, Q. WANG and Q. XUE, *Nucl. Inst. Meth. Phy. Res.* B **143** (1998) 488.
18. E. SMETHURST and R. B. WATERHOUSE, *J. Mater. Sci.* **12** (1977) 1781.
19. W. C. OLIVER and G. M. PHARR, *J. Mat. Res.* **7** (1992) 1564.
20. J. F. ZIEGLER, J. P. BIERSACK and U. LITTMARK, "The Stopping and Range of Ions in Solids" (Pergamon, New York, 1985).
21. B. J. INKSON, *Acta Mater.* **48** (2000) 1883.
22. L. PRANEVICIUS, K. F. BADAWI, N. DURAND, J. DELAFORD and P. GOUDEAU, *Surf. Coat. Technol.* **71** (1995) 254.
23. H. Z. WU, C. W. LAWRENCE, S. G. ROBERTS and B. DERBYTHE, *Acta Mater.* **46** (1998) 383.
24. L. LAWRENCE, L. LIL and J. T. SPENCER, *Surf. Coat. Technol.* **115** (1999) 273.
25. T. HIOKI, A. ITOH, M. OHKUBO, S. NODA, H. DOI, J. KAWAMOTO and O. KAMIGAITO, *J. Mater. Sci.* **21** (1986) 1321.
26. C. J. McHARGUE, C. W. WHITE, B. R. APPLETON, G. C. FARLOW and J. M. WILLIAMS, *Mater. Res. Soc. Symp. Proc.* **27** (1984) 385.
27. F. HALITIM, S. PALETTO, G. FANTOZZI and D. TREHEUX, *J. Eur. Ceram. Soc.* **15** (1995) 833.
28. S. B. NEWCOMB, *Private Commun.* (2001).
29. C. J. McHARGUE, *Mater. Sci. Eng.* A **253** (1998) 94.
30. P. J. BURNETT and T. F. PAGE, *J. Mater. Sci.* **20** (1985) 4624.
31. L. BOUDOUKHA, S. PALETTO and G. FANTOZZI, *Nucl. Inst. Meth. Phy. Res.* B **108** (1996) 87.
32. H. G. JANG, H. B. KIM, J. H. JOO, C. N. WHANG, H. K. KIM, D. W. MOON, J. J. WOO and S. O. KIM, *Nucl. Inst. Meth. Phy. Res.* B **124** (1997) 528.
33. C. J. McHARGUE, G. C. FARLOW, C. W. WHITE, J. M. WILLIAMS, B. R. APPLETON and H. NARAMOTO, *Mater. Sci. Eng.* **69** (1985) 123.
34. S. J. BULL and T. F. PAGE, *J. Mater. Sci.* **23** (1988) 4217.
35. L. CLICHE, S. ROORDA and R. A. MASUT, *Nucl. Inst. Meth. Phy. Res.* B **96** (1995) 319.
36. L. M. HOWEY and M. H. RAINVILLE, *ibid.* **19/20** (1987) 61.
37. P. J. BURNETT and T. F. PAGE, *Amer. Ceram. Soc. Bull.* **65** (1986) 1393.
38. L. BOUDOUKHA, S. PALETTO, F. HALITIM and G. FANTOZZI, *Nucl. Inst. Meth. Phy. Res.* B **122** (1997) 233.
39. Y. MIYAGAWA, S. NAKAO, K. BABA, R. HATADA, M. IKEYAMA and S. MIYAGAWA, *Surf. Coat. Technol.* **103/104** (1998) 323.
40. K. E. SICKAFUS, H. MATZKE, T. HARTMANN, K. YASUDA, J. A. VALDEZ, P. CHODAK, M. NASTASI and R. A. VERRALL, *J. Nucl. Mater.* **274** (1999) 66.
41. N. SASAJIMA, T. MATSUI, K. HOJOU, S. FURUNO, H. OTSU, K. IZUI and T. MUROMURA, *Nucl. Inst. Meth. Phy. Res.* B **141** (1998) 487.
42. L. M. WANG, S. X. WANG, S. ZHU and R. C. EWING, *J. Nucl. Mater.* **289** (2001) 122.
43. M. E. MURPHY, Thesis: The Use of Ion Implantation for Biomedical Applications, University of Limerick, Ireland, 2002.
44. C. PICONI, W. BURGER, H. G. RICHTER, A. CITTADINI, G. MACCAURO, V. COVACCI, N. BRUZZESE, G. A. RICCI and E. MARMO, *Biomaterials* **19** (1998) 1489.
45. T. K. GUPTA, F. F. LANGE and J. H. BECHTOLD, *J. Mater. Sci.* **13** (1978) 1464.

Received 2 April 2002
and accepted 18 September 2003